An experimental study of phase equilibria and Fe oxy-component in kaersutitic amphibole: Implications for the f_{H_2} and a_{H_2O} in the upper mantle

Robert K. Popp

Department of Geology and Geophysics, Texas A&M University, College Station, Texas 77843, U.S.A.;
and Center for High Pressure Research, 5251 Broad Branch Road NW, Washington, DC 20015, U.S.A.

David Virgo

Geophysical Laboratory and Center for High Pressure Research, 5251 Broad Branch Road NW, Washington, DC 20015, U.S.A.

Hatten S. Yoder, Jr., Thomas C. Hoering

Geophysical Laboratory, 5251 Broad Branch Road NW, Washington, DC 20015, U.S.A.

Michael W. Phillips

Department of Geology, University of Toledo, Toledo, Ohio 43606, U.S.A.

Abstract

Experiments have been carried out from 500 to 1200 °C, 1 atm to 10 kbar, and f_{H_2} from that of the IQF buffer to air, to quantify the variation of Fe oxy-component content in a titanian pargasite megacryst amphibole from Vulcan's Throne, Arizona. The results document the operation of the following substitution mechanism in the amphibole crystal structure: $Fe^{2+} + OH^- = Fe^{3+} + O^{2-} + \frac{1}{2}H_2$ whereby the Fe^{3+}/Fe_{tot} of the amphibole is controlled by T, P, and f_{H_2}. For the amphibole composition that was investigated, there is a linear variation of log f_{H_2} as a function of log (Fe^{3+}/Fe^{2+}) at fixed T and P of the form log $f_{H_2} = a + b \log(Fe^{3+}/Fe^{2+})$. Values of a and b are:

T (°C)	P (kbar)	a	b
700	1	−2.66	−5.14
800	1	−1.84	−4.31
900	1	−1.01	−3.76
1000	1	−0.30	−3.95
900	5	−0.70	−4.69
900	10	−0.50	−4.60

Two different expressions were defined for the equilibrium constant for the amphibole Fe end-member reaction $Ca_2Fe_5^{2+}Si_8O_{22}(OH)_2 = Ca_2Fe_3^{2+}Fe_2^{3+}Si_8O_{24} + H_2$. In the random mixing model, in which it is assumed that Fe^{3+} and Fe^{2+} mix randomly on the five M1, M2, and M3 crystallographic sites,

$$K = f_{H_2}(28.94)\frac{(X_{Fe^{3+}})^2(X_{[]})^2}{(X_{Fe^{2+}})^2(X_{OH})^2}$$

for which

$$\log K = 4.25 - 4363/T \text{ (K)} + 0.11(P - 1) \text{ (kbar)}.$$

From the appropriate values of K, f_{H_2} of the experiments can be predicted to within ~0.5 log units from knowledge of the absolute amounts of Fe^{3+}, Fe^{2+}, and OH in the amphibole. For the nonrandom mixing model, in which observed Fe^{3+} and Fe^{2+} site populations are used to define the mole fraction terms,

$$K = f_{H_2}(28.94)\frac{(X_{Fe^{3+}}^{M1})^{0.8}(X_{Fe^{3+}}^{M2})^{0.8}(X_{Fe^{3+}}^{M3})^{0.4}(X_{[]})^2}{(X_{Fe^{2+}}^{M1})^{0.8}(X_{Fe^{2+}}^{M2})^{0.8}(X_{Fe^{2+}}^{M3})^{0.4}(X_{OH})^2}$$

for which

$$\log K = 5.29 - 5903/T \text{ (K)} + 0.13(P - 1) \text{ (kbar)}.$$

With this model, f_{H_2} of the experiments can be predicted to within ~0.3 log units from knowledge of the relevant ionic contents. The random mixing model yields slightly poorer

estimates of f_{H_2} but can be used for literature data in applications because Fe^{3+} and Fe^{2+} site populations for natural kaersutite are seldom reported. In order to use the K expressions, the OH content of the amphibole must be known. In kaersutite for which H content has not been measured, OH apfu can be estimated as $(2.0 - Fe^{3+} - Ti)$.

Because both the reactant and product amphiboles in the end-member reaction refer to components in a single homogenous amphibole phase, the K expressions should apply to any calcic amphibole in which Fe^{3+} and Fe^{2+} mix on the five M1, M2, and M3 crystallographic sites, regardless of the amphibole bulk composition.

The study confirms that the relatively high Fe^{3+}/Fe_{tot} of most natural kaersutitic amphiboles can result from P-T-f_{H_2} conditions characteristic of the upper mantle, rather than from oxidation during ascent or eruption. Closed-system cooling favors the reduction, not oxidation, of amphibole. With K values from the equations above, it is possible to predict f_{H_2} of amphibole crystallization, presumably from a melt, if P and T, as well as the relevant amphibole composition terms, are known. Calculated values of f_{H_2} for the majority of kaersutitic amphiboles reported in the literature range from approximately 0.01 to 100 bars. Such f_{H_2} values are generally consistent with estimated redox states and H_2O activities of mantle processes. If f_{H_2} estimates are combined with f_{O_2} estimates made on the same xenolith assemblages, H_2O activity in the environment of formation can be predicted.

INTRODUCTION

Amphibole has been widely recognized in mantle xenoliths that are entrained in both alkali basalts and kimberlites. The mineral has attracted the attention of petrologists ever since Oxburgh (1964) suggested that its presence as a phase in the upper mantle would explain the high K content of mantle-derived basalts. Recently, it has been accepted that the introduction of hydrous phases, both amphibole and mica, into a refractory mantle (referred to as modal metasomatism, Harte, 1983; Dawson, 1984) would account for the reenrichment in the major elements (Ti, Fe, K, and P) that were lost in previous melting events.

The chemical variability of amphibole in mantle samples has been summarized by Best (1970), Dawson and Smith (1982), and Wilkinson and LeMaitre (1987). Alkali basalt associations are generally characterized by Ti-rich hornblendes such as titanian pargasite or kaersutite. These amphiboles occur as mono-mineralic megacrysts and as one of the phases in Type I and Type II spinel peridotite assemblages (e.g., Wilshire and Shervais, 1975; Frey and Prinz, 1978). Amphibole also occurs in Type II assemblages as veins, selvages, and dikes cross-cutting Type I peridotite. In xenolith assemblages, amphibole occurs in a variety of textural relationships ranging from primary metasomatic replacement textures to intercumulus textures. Wilshire et al. (1988) gave a comprehensive review of the occurrence, mineralogy, textures, and chemical data for amphibole-bearing xenoliths associated with alkalic volcanism of the Western U.S.

Kaersutitic amphiboles also occur in magmatic inclusions in SNC-type meteorites, which are considered to have originated on the planet Mars (Treiman, 1985; Johnson et al., 1991; Harvey and McSween, 1992). The mineral assemblages contained in these meteorite types are notable because they provide insight into magmatic processes on planets other than Earth.

Models for the petrogenesis of amphiboles in alkalic associations have been proposed by Wilkinson and LeMaitre (1987). Interstitial amphiboles may be the products of near-iso-chemical hydration reactions in which anhydrous peridotite minerals react with fluid to form amphibole (e.g., Best, 1974; Francis, 1976; Kurat et al., 1980; Griffen et al., 1984; Nickel and Green, 1984; Wilkinson and LeMaitre, 1987; Schneider and Eggler, 1984; Wallace and Green, 1991). In contrast, the origin of the poikilitic, vein, and megacryst amphiboles most likely involves crystallization of silicate melts at high pressure (e.g., Binns et al., 1970; Irving and Frey, 1984; Merrill and Wyllie, 1975).

Although there have been extensive studies of the compositions, textural relationships, and tectonic settings of Ti-bearing amphiboles, the phase relations of these amphiboles are poorly understood. As summarized by Helz (1982), a number of experimental studies have investigated the melting relations of amphiboles in natural rock compositions with and without modal amphibole. Studies of the stability of titanian pargasite or kaersutite amphiboles at supersolidus conditions include studies in fluid absent $(P_{H_2O} < P_{tot})$ systems on kaersutite samples from the Hocheifel tertiary volcanic field (Huckenholz et al., 1992); from Black Rock Summit, southwestern U.S.A., and Iki Island, Japan (Oba et al., 1983); and from Kakanui, New Zealand (Merrill and Wyllie, 1975). Fluid excess $(P_{H_2O} = P_{tot})$ experiments have been carried out on a kaersutite megacryst from Kakanui, New Zealand, and a megacryst from Dish Hill (Stewart et al., 1979). Johnson et al. (1991) carried out melting experiments on the composition 50% Fe-Ti basalt, 50% kaersutite under f_{O_2} buffered conditions of both $P_{H_2O} = P_{tot}$ and $P_{H_2O} < P_{tot}$. Despite the general success of the existing experimental data in defining the stability of amphibole at supersolidus conditions, most experiments have not been carried out under f_{H_2}/f_{O_2} controlled conditions in the melting region, nor have the bulk chemical compositions, Fe^{3+}-Fe^{2+} ra-

A. 90 Kaersutitic Amphiboles

Frequency

Fe³⁺ / Fe$_{total}$

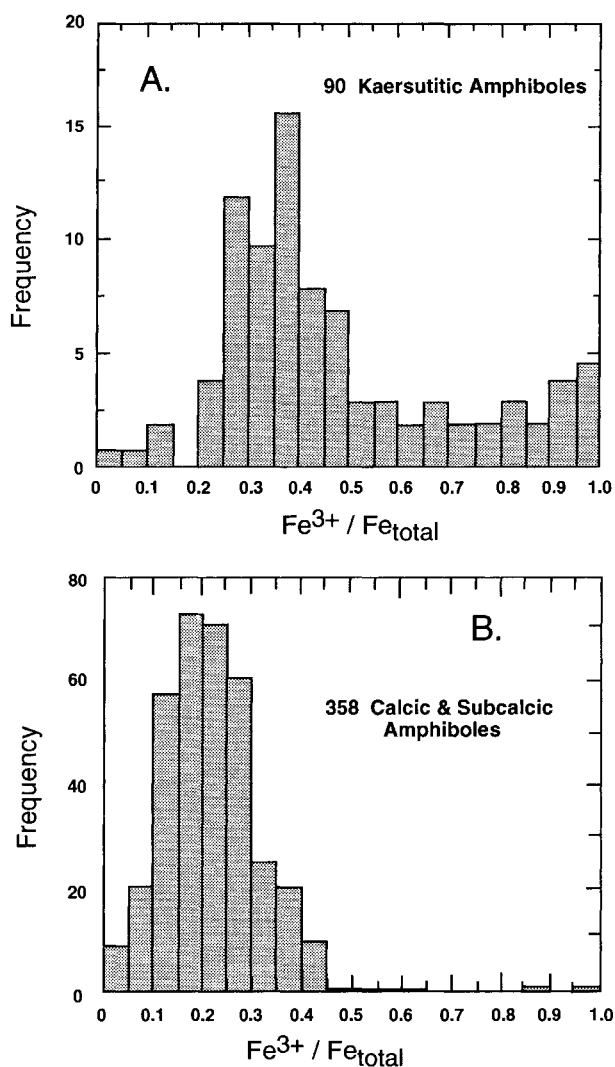## B. 358 Calcic & Subcalcic Amphiboles

Frequency

Fe³⁺ / Fe$_{total}$

Fig. 1. (A) Frequency histogram of Fe^{3+}/Fe_{tot} for 90 kaersutitic amphiboles from inclusions in alkali basalts. Data from Popp and Bryndzia (1992, 70 samples) and Dyar et al. (1993, 20 samples). (B) Frequency histogram of Fe^{3+}/Fe_{tot} for 358 calcic and subcalcic amphiboles, excluding kaersutitic varieties. Data from Leake (1968).

tios, or H_2O^+ contents of the amphibole experimental products been systematically determined. Thus, a direct comparison between the compositions of the natural amphibole and those of the experimental products is not possible.

Kaersutitic amphiboles have an unusual crystal chemistry that is related to their Fe^{3+}, Ti, and volatile contents. Overall, these amphiboles have high $Fe^{3+}-Fe^{2+}$ ratios, as well as variable H_2O^+ contents, such that the sum of (OH + F + Cl) is generally less than the ideal 2.0 atoms per formula unit (apfu). The highly oxidized nature of Fe in these amphiboles has been well documented since the early studies of natural samples (e.g., Aoki, 1963; Boettcher and O'Neil, 1980; Irving and Frey, 1984). A

frequency histogram of the Fe^{3+}/Fe_{tot} of approximately 90 natural samples compiled by Popp and Bryndzia (1992) and Dyar et al. (1993) is shown in Figure 1A. The observed $Fe^{3+}-Fe^{2+}$ ratios span nearly the entire range from 0.0 to 1.0, but many of the amphiboles are relatively more oxidized than calcic amphiboles from other environments (see Fig. 1B). Recent documentation of an inverse 1:1 correlation between Fe^{3+}- and H-content in naturally occurring megacryst amphiboles (Popp and Bryndzia, 1992; Dyar et al., 1993; Virgo et al., 1994) requires that essentially all the Fe^{3+} is accommodated by an oxy-component described in the charge-balanced oxidation-dehydrogenation reaction,

$$Fe^{2+} + OH^- = Fe^{3+} + O^{2-} + \frac{1}{2}H_2. \qquad (1)$$
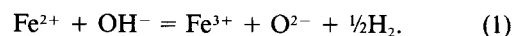
Thus, accommodation of Fe^{3+} by components such as ferri-tschermakite or magnesio-riebeckite is not significant in these amphiboles. Substitution 1 has also been documented in experimentally treated kaersutitic amphibole (Virgo et al., 1994). Furthermore, on the basis of principle components analysis of the chemical compositions of 90 natural kaersutitic amphiboles, Virgo et al. (1994) have concluded that Ti is accommodated primarily by a multivariate substitution that involves Ti and OH in 1:−1 proportions. Therefore, the simultaneous operation of the two oxy-amphibole substitution mechanisms exerts significant control over the crystal chemistry of kaersutitic amphiboles, such that the deficiency of H, relative to the theoretical value of 2.0, is equal to the sum of both the Fe^{3+} and Ti occupancy expressed on an atoms per formula unit basis.

Consideration of the likely diffusion rates of H in amphibole (Dyar et al., 1993) and the preliminary experimental results of amphibole stability (Popp et al., 1993) has recently cast doubt on the notion that kaersutitic amphiboles have undergone extensive oxidation-dehydrogenation during ascent and eruption. In addition, the use of amphibole volatile contents to infer information on H_2O activity in the environment of crystallization (e.g., Treiman, 1985; Harvey and McSween, 1992) may be tenuous in light of the strong crystal chemical control of Fe^{3+} and Ti on H content.

This study reports the results of phase equilibrium experiments, primarily in the subsolidus region, for a sample of titanian pargasite megacryst entrained within an alkali basalt from Vulcan's Throne, Arizona. Experiment conditions ranged from 1 atm to 10 kbar, 500 to 1200 °C, and f_{H_2} from that of air to that defined by the IQF solid state buffer.

PROCEDURES

Starting material

The amphibole sample used in the experiments, a titanian pargasite from Vulcan's Throne, Arizona (National Museum of Natural History sample no. 122377), was obtained through the courtesy of P. Dunn of the Smithsonian Institution. Chips from five individual megacrysts from that locality were analyzed with the electron micro-

TABLE 1. Electron microprobe analyses (weight percent oxides) of amphibole starting material and selected experimental products

	Vulcan's Throne titanian pargasite ($\pm 1\sigma$ for 210 grains)	700 °C Air 2 h	700 °C Air 4 h	700 °C IQF	1 kbar 800 °C HM	1 kbar 800 °C NNO	1 kbar 900 °C HM	10 kbar 900 °C FMQ
SiO_2	40.32(0.20)	40.24	40.27	40.05	40.31	40.03	40.34	39.89*
TiO_2	3.84(0.17)	3.86	3.87	3.79	3.85	3.91	3.96	3.96
Al_2O_3	15.35(0.14)	15.47	15.58	15.37	15.43	15.48	15.43	15.26
Cr_2O_3	BDL**	BDL	BDL	BDL	BDL	BDL	BDL	BDL
MgO	14.53(0.14)	14.62	14.62	14.62	14.70	14.62	14.73	14.61
CaO	10.46(0.14)	10.47	10.54	10.45	10.45	10.49	10.49	10.50
MnO	BDL	BDL	BDL	BDL	BDL	BDL	BDL	BDL
FeO†	7.70(0.18)	7.69	7.71	7.67	7.84	7.69	7.71	7.72
NiO	BDL	BDL	BDL	BDL	BDL	BDL	BDL	BDL
ZnO	BDL	BDL	BDL	BDL	BDL	BDL	BDL	BDL
Na_2O	2.74(0.05)	2.75	2.73	2.78	2.79	2.80	2.79	2.76
K_2O	1.60(0.06)	1.60	1.61	1.61	1.64	1.60	1.59	1.60
F‡	0.08(0.03)	0.07	0.08	0.08	0.09	0.08	BDL	BDL
Cl	BDL	BDL	BDL	BDL	BDL	BDL	BDL	BDL

* The value of 1σ for SiO_2 is 0.43.
** BDL = below detection limit.
† Total Fe as FeO.
‡ F contents are at detection limits.

probe to assess their homogeneity. Point analyses for 14 elements were made at ~0.25 mm intervals in two directions at approximately right angles on each chip. Although small areas of heterogeneity, probably inclusions of pyroxene, were encountered in some of the chips, there was not significant variation in the composition of the amphibole. One of the megacrysts with only minor inclusions was selected as the starting material. The sample was crushed and washed in alcohol. A magnetic fraction, mostly consisting of grains with an oxidized coating, was removed with the Franz Isodynamic Separator. The remaining sample, weighing ~11 g, was sieved into three fractions: 80–120, 120–170, and 170–230 openings/in. Electron microprobe analyses were made on a single point in the center of each of 70 randomly selected grains in each of the three sieved fractions. The mean and standard deviation values of oxide contents for all 210 analyses (Table 1) confirm that the starting material was homogenous. The oxide weight percents in Table 1 were used to calculate the composition of the Vulcan's Throne amphibole expressed in atoms per formula unit normalized to 24 anions pfu (see Table 2). The H contents and Fe^{3+}-Fe^{2+} ratios required for the calculation were obtained from Table 3.

Phase identification and characterization

The starting amphibole and experimental products were analyzed thoroughly by petrographic analysis, powder X-ray diffraction, electron microprobe analysis, and [57]Fe Mössbauer spectroscopy. A vacuum fusion, U-furnace, manometry system was used to analyze the H-contents of the natural amphibole and selected experimental products. Electron microprobe analyses and SEM observations were carried out on both the Cameca SX50 instrument at the Department of Geology at Texas A&M University, and the JEOL JXA-8800L instrument at the Geophysical

Laboratory. The agreement between the analyses obtained by the two instruments is excellent. The Mössbauer spectroscopy and H-analyses were carried out at the Geophysical Laboratory. The details of those techniques are described elsewhere (Young et al., in preparation). The compositions of the starting amphibole and selected experimental product amphiboles are given in Table 1.

Apparatus

The air-heating experiments were carried out in either a Lindberg muffle furnace or a Pt-wound quenching furnace. The muffle furnace was calibrated with the same temperature-measuring system used in the 1 kbar hydrothermal experiments.

The 1 kbar experiments at 800 °C and below were carried out in horizontally mounted, Rene-41 cold-seal pressure vessels at the Geology Department at Texas A&M University. The system is similar in design to that depicted by Ernst (1968, Fig. 16). Calibration of the system has been described in detail by Clowe et al. (1988).

The 5 and 10 kbar experiments, as well as the 1 kbar experiments at temperatures above 800 °C, were carried

TABLE 2. Chemical composition of Vulcan's Throne amphibole

Si	5.97
Ti	0.42
Al	2.07
Mg	3.23
Ca	1.66
Fe^{2+}	0.65
Fe^{3+}	0.30
Na	0.79
K	0.30
H	1.26

Note: values tabulated are atoms per formula unit normalized to 24 anions pfu. Elements at or below the detection limit in Table 1 are neglected.

TABLE 3. Experimental results

T (°C)	t	Buffer	Initial R*	Final R	wt% H_2O	log f_{H_2}	log f_{O_2}
Natural starting material							
			0.317		1.27		
Air-heating experiments							
1000	4 h		0.317	1.00			
1000	24 h		0.317	1.00			
1000	7 d		0.317	1.00			
800	24 h		0.317	1.00			
800	4 h		0.317	1.00			
700	6 d		0.317	1.00			
700	2 d		0.317	1.00	0.55		
700	24 h		0.317	0.931			
700	4 h		0.317	0.691	0.89		
700	4 h		0.317	0.609			
700	2 h		0.317	0.535	1.02		
700	1 h		0.317	0.439	1.14		
700	0.5 h		0.317	0.390	1.14		
500	24 h		0.317	0.342			
500	4 h		0.317	0.320			
1 kbar hydrothermal experiments							
1000	12 h	HM	0.317	0.662		−1.46	−5.5
1000	2 h	NNO	1.000	0.344		0.89	−10.19
1000	1.5 h	NNO	0.317	0.323		0.89	−10.19
900	1 d	HM	0.317	0.577		−1.46	−7.21
900	2 d	HM	0.317	0.558		−1.46	−7.21
900	12 h	FMQ	0.317	0.201		1.19	−12.52
900	12 h	NNO	0.317	0.250		0.85	−11.85
800	3 d	HM	0.691	0.453	1.24	−1.58	−9.25
800	2 d	HM	0.317	0.480		−1.58	−9.25
800	2 d	NNO	0.317	0.198	1.42	0.71	−13.83
800	1 d	FMQ	0.317	0.181		1.06	−14.53
800	2 d	GM	0.317	0.099	1.37	2.27	−17.08
800	2 d	GM	0.071	0.104	1.43	2.27	−17.08
800	11 h	IQF	0.317	0.065	1.53	2.99	−19.82
700	7 d	HM	0.317**	0.408	1.32	−1.75	−11.70
700	7 d	HM	0.691	0.406		−1.75	−11.70
700	7 d	HM	0.317	0.396	1.25	−1.75	−11.70
700	7 d	HM	0.317	0.387	1.12	−1.75	−11.70
700	7 d	NNO	0.317	0.179		0.51	−16.21
700	7 d	FMQ	0.317	0.179		0.87	−16.94
700	1 d	GM	0.317	0.129		1.99	−19.25
700	14 d	GM	0.317	0.114	1.43	1.99	−19.25
700	6 d	GM	0.071	0.112		1.99	−19.25
700	2 d	GM	0.317	0.117		1.99	−19.25
700	7 d	GM	0.317	0.105		1.99	−19.25
700	6 d	GM	0.317	0.102	1.43	1.99	−19.25
700	11 h	IQF	0.317	0.071	1.53	3.00	−22.63
600	11 d	HM	0.691	0.364		−1.92	−14.71
600	11 d	HM	0.317	0.321	1.26	−1.92	−14.71
600	11 d	NNO	0.317	0.186	1.37	0.29	−19.14
600	10 d	GM	0.317	0.146	1.41	1.67	−21.93
600	13 h	IQF	0.317	0.119	1.50	3.02	−26.08
500	11 d	HM	0.691	0.336	1.23	−2.02	−18.51
500	10 d	HM	0.317	0.288	1.33	−2.02	−18.51
500	10 d	GM	0.317	0.224	1.35	1.37	−25.30
500	10 d	NNO	0.317	0.220	1.33	0.14	−22.83
500	1 d	IQF	0.317	0.174		3.06	−30.43
500	11 d	HM	0.112	0.166		−2.02	−18.51
5 kbar hydrothermal experiments							
900	24 h	HM	0.317	0.530		−0.74	−7.15
900	12 h	FMQ	0.317	0.240		1.78	−12.20
10 kbar hydrothermal experiments							
900	24 h	HM	0.317	0.492		−0.25	−7.07
900	12 h	FMQ	0.317	0.223		2.12	−11.80

* R = Fe^{3+}/Fe_{tot} obtained from Mössbauer spectra as described by Young et al. (in preparation). Error of measurement is ±3% (relative).
** Starting material was well-ground.

out in the internally heated, Ar gas apparatus at the Geophysical Laboratory (Yoder, 1950).

Experimental techniques

For the air-heating experiments, the amphibole charge was loaded into an Au or Pt boat, which was then placed into the furnace. At the termination of experiments in the muffle furnace, the sample container was removed from the furnace and cooled to room temperature over the course of ~3–5 min. Experiments in the quenching furnace were terminated by completing the electrical connection through the support wire that held the sample container. The wire thereby melted, and the container dropped into a beaker of distilled water; quench time to room temperature was probably on the order of several seconds.

Hydrogen fugacity in the hydrothermal and internally heated apparatus experiments was controlled with the standard solid buffer techniques (e.g., Huebner, 1971; Chou, 1987b). The hematite + magnetite (HM), nickel + nickel oxide (NNO), fayalite + magnetite + quartz (FMQ), and iron + quartz + fayalite (IQF) buffers were used in both types of apparatus, whereas the graphite + methane (GM) buffer was used in only the hydrothermal apparatus. In buffered experiments, approximately 0.10 g of amphibole plus 7–20 mg of distilled-deionized water were sealed into an inner $Ag_{70}Pd_{30}$ or Pt capsule (3.1 cm × 3.0 mm o.d. × 2.4 mm i.d.). The inner capsule was sealed into an outer Au capsule (3.81 cm × 4.75 mm o.d. × 4.0 mm i.d.) containing approximately 0.25 g of the buffer assemblage and 15–75 mg of distilled-deionized water. For experiments made at the graphite + methane buffer, the sealed, Ag-Pd capsule was loaded directly into the vessel with a small graphite filler rod, and the system was pressurized with methane.

Upon completion of the hydrothermal experiments, the vessels were removed from the furnaces and quenched in a stream of compressed air. The vessels reached a temperature of <80 °C in a maximum of 8 min. To terminate the experiments carried out in the gas apparatus, the power was turned off, and the quench required <2 min.

After opening the capsules, the presence of H_2O in both the buffer and charge was verified by heating a portion of the charge for several minutes at ~150 °C in a small bottle on a hot plate and noting the condensation on the upper walls of the bottle.

Experiment times varied from 30 min to 11 d. Products of some experiments were reused at different conditions in order to document that equilibrium Fe^{3+}-Fe^{2+} ratios were achieved by means of reversed experiments.

RESULTS

The results of the subsolidus experiments are given in Table 3, which lists the temperature, pressure, duration, buffer assemblage, initial and final Fe^{3+}-Fe^{2+} ratio of the amphibole, OH content of the amphibole, and log of the equilibrium f_{H_2} and f_{O_2} of the experiments. The results of experiments undertaken to locate the solidus in a semi-

TABLE 4. Activity coefficients for gases*

T (°C)	P (kbar)	H_2O	H_2
500	1	0.453	1.32
600	1	0.636	1.27
700	1	0.767	1.23
800	1	0.853	1.20
900	1	0.909	1.18
1000	1	0.944	1.16
900	5	1.03	2.21
900	10	1.78	4.26
900	15	3.38	7.15
1000	15	3.39	5.93

* Calculated with the computer program of Lamb and Valley (1984).

Fig. 2. Variation in Fe^{3+}/Fe_{tot} as a function of temperature at 1 kbar in experimentally treated Vulcan's Throne titanian pargasite. Symbols represent experiments buffered by the following assemblages. Solid circles: HM; open circles: NNO; squares: FMQ; triangles: GM. For symbols not highlighted with an arrow, starting material was the natural sample, the Fe^{3+}/Fe_{tot} of which is indicated by the dashed line. The Fe^{3+}/Fe_{tot} of the starting material for symbols with arrows is indicated adjacent to the arrow. Error in measurement of Fe^{3+}/Fe_{tot} is 0.01–0.02. Shaded area represents conditions for which reaction rates were inadequate for a close approach to equilibrium during the experiments.

quantitative manner are not tabulated but are discussed below.

The experiments listed in Table 3 provide no evidence of decomposition of the amphibole to other phases. This conclusion is based on X-ray, optical, SEM, and electron microprobe analyses of the starting material and experimental products. Observation of grain mounts in oils revealed no significant differences between the initial and final amphibole other than changes in the optical properties consistent with the operation of Reaction 1. Within $\pm 2\sigma$, there is no difference between the chemical compositions of the initial and final amphiboles (Table 1). Electron microprobe point scans of the experimental products from edge to opposite edge of the amphibole grains revealed no zoning within the precision of measurement. The SEM images of the surfaces of these amphibole grains revealed no evidence of significant decomposition. For example, the sample that was air-heated at 700 °C for 4 h contained widespread, but highly scattered, thin films of an Fe-rich phase (probably iron oxide) on the amphibole surfaces. Substantial iron oxide phases resulting from amphibole decomposition, such as those observed by Phillips et al. (1991), were not identified. In support of that observation, the composition of the 700 °C, 4 h experimental product (Table 1) is not different from that of the starting amphibole, nor was an iron oxide phase detected in the Mössbauer spectrum. Both the electron microprobe and petrographic analyses of amphibole in the experimental products verify that the loss of Fe to capsule material was not significant in the few experiments in which Pt capsules were used. Thus, with the exception of the change of oxidation state of Fe, and the loss of H as prescribed by Reaction 1, there is no observable change in amphibole composition in any of the experiments reported in Table 3.

One aspect of the amphibole analyses requires additional explanation. After the weight percent oxides are corrected for the amounts of Fe^{3+} and H, the weight percent totals obtained from both the Cameca and JEOL instruments are in the range 98.0–98.5. The low totals relative to 100% may result from differences in the degree of rounding or quality of polish between the standards and small-sized amphibole samples, or from incorrect matrix correction factors applied in the data reduction.
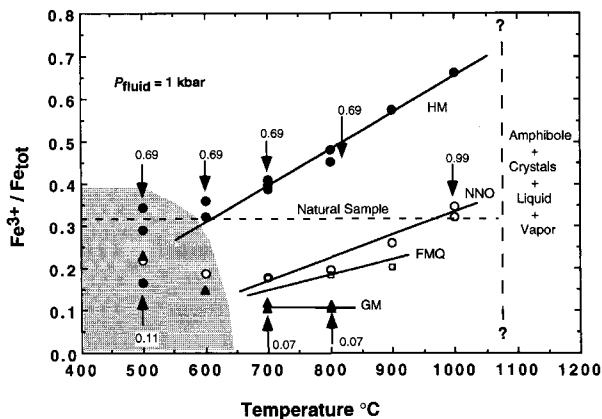
In either case, the purpose of the microprobe analyses is to evaluate the extent, if any, of the decomposition of the experiment-product amphiboles. Therefore, the low oxide totals for both the starting and product amphiboles are considered adequate for documenting constant amphibole composition.

For all the buffers except GM, values for the f_{O_2} reported in Table 3 were calculated from the equations given by Chou (1987b). The corresponding f_{H_2} values of the buffers were calculated from the f_{O_2} values by means of the dissociation constant for H_2O (Robie et al., 1978) and based on the assumption that $P_{fluid} = P_{H_2O} + P_{H_2} + P_{O_2}$ (Eugster and Skippen, 1967). Activity coefficients (listed in Table 4) for pure H_2 and pure H_2O were calculated using the computer program of Lamb and Valley (1984), which employs a hard-sphere, Modified Redlich-Kwong equation of state. In the case of the GM buffer, f_{H_2} values were obtained from a least squares fit of the values tabulated by Eugster and Skippen (1967, Table 1), which are in excellent agreement (within 0.01–0.02 log units) with those calculated for the GM buffer by the Lamb and Valley (1984) computer program. It should be noted, however, that Chou (1987a) measured f_{H_2} values 0.3–0.6 log units lower than those calculated for the GM buffer at 2 kbar in the range 650–800 °C. Values of f_{O_2} reported for the GM buffer in Table 3 were calculated in a manner analogous to that described above for calculating f_{H_2} values from the f_{O_2} values for the other buffers.

The results of the 1 kbar hydrothermal experiments are plotted in Figure 2, which shows the variation in Fe^{3+}/Fe_{tot} of the amphibole products as a function of temper-
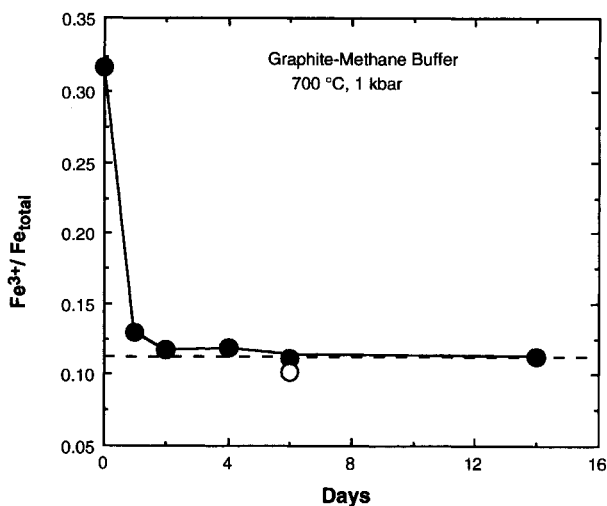
Fig. 3. Variation of Fe^{3+}/Fe_{tot} as a function of time for experiments carried out on the Vulcan's Throne amphibole at 700 °C, 1 kbar, and f_{H_2} controlled by the GM buffer. Solid circles indicate experiments starting with the natural sample. Open circle indicates a reversal experiment that started with a previously reduced sample ($Fe^{3+}/Fe_{tot} = 0.07$). Uncertainty in Fe^{3+}/Fe_{tot} is 0.01–0.02. Dashed line represents mean value of all experiments of 2 d or longer.

ature for experiments at the HM, NNO, FMQ, and GM buffers. The results at the lowest f_{O_2} buffer, IQF, are not plotted because reversal of equilibrium cannot be documented by experiments starting with more reduced amphibole. Amphibole products from the IQF buffer, however, were used as starting materials for reversals to document equilibrium at the GM buffer.

A series of nonreversed experiments was carried out in air and at 1 kbar to define the onset of the decomposition or melting of the Vulcan's Throne amphibole. In air-heating experiments, no observable changes occurred in 7-d experiments at 1000 °C (Table 3). Subsolidus decomposition of the amphibole occurred within the range 1050–1100 °C, whereas melting was observed at 1125 °C and higher. Hydrous amphiboles may be unstable in air, but oxy-amphibole with 100% Fe^{3+} may possibly be a stable phase in air. At 1 kbar and the HM buffer, glass and nonamphibole crystalline phases were produced at 1100 °C, whereas at 1050 °C there was no distinct evidence for either melting or decomposition in experiments lasting 3 h. At the NNO buffer, 1000 °C experiments did not produce melting, but at 1084 °C melting had clearly taken place. On the basis of these experiments, an isothermal boundary for the amphibole + crystals + liquid + vapor field has been drawn in Figure 2 at a temperature between 1050 and 1100 °C. This solidus curve is located approximately 100–125 °C higher than the curves reported at 1 kbar by Johnson et al. (1991) and Huckenholz et al. (1992). Those studies, however, were carried out either on a bulk composition of kaersutite + basalt or at $P_{H_2O} < P_{tot}$, conditions under which a lower thermal stability of amphi-

bole might be expected. Thus, the results are not directly comparable to those of this study.

Information on the kinetics of the Fe oxy-substitution mechanism can be obtained from the experimental results. In any buffered experiment, however, the equilibration time is related not only to the kinetics of the reaction under investigation but also to the rate of H diffusion through the capsule walls. Under conditions of the NNO buffer at 1000 °C and 1 kbar, a close reversal of equilibrium Fe^{3+}/Fe_{tot} was achieved in 1.5 h (Fig. 2). Figure 3 is a plot of Fe^{3+}/Fe_{tot} vs. time for experiments made at the GM buffer at 700 °C and 1 kbar. It is evident from these results that the equilibrium Fe^{3+}/Fe_{tot} value was achieved in ~2 d. At temperatures of 600 °C and below (shaded area in Fig. 2), reaction rates are much more sluggish, and so for the NNO and GM buffers equilibrium was not approached in experiments lasting up to 11 d. At 500 °C, heating in air for 24 h produced little or no change in Fe^{3+}/Fe_{tot}, given the uncertainty of measurement (Table 3), whereas at 700 °C significant change was observed after only 0.5 h of air heating. Thus, it is concluded that the rate of the Fe oxy-reaction decreases substantially upon cooling below ~700 °C.

For each buffer, there is a linear variation of Fe^{3+}/Fe_{tot} in the amphibole as a function of temperature (Fig. 2). Similar behavior has been observed in synthetic biotite (Redhammer et al., 1993) but is contrary to observations of intrinsic f_{O_2} made for melts (e.g., Carmichael, 1991) and whole-rock systems (e.g., Ulmer et al., 1976), in which the oxidation state of Fe remains essentially constant along a single buffer curve as temperature varies. The temperature dependence of Fe^{3+}/Fe_{tot} in the Vulcan's Throne amphibole decreases as the buffer assemblages become more reducing, such that the slopes of the best-fit lines decrease systematically from the HM to GM buffers (Fig. 2). The latter behavior is not related to the effects of the buffer assemblages because the changes in both f_{H_2} and f_{O_2} as a function of temperature in the 700–1000 °C range are essentially identical for the HM, NNO, and FMQ buffers (see Table 3). The change in f_{H_2} and f_{O_2} for the GM buffer between 700 and 1000 °C is approximately double that of the more oxidizing buffers, but Fe^{3+}/Fe_{tot} in the amphibole remains essentially constant over that temperature range (Fig. 2).

Figure 4 is a plot of log f_{H_2} of the experiments vs. log (Fe^{3+}/Fe^{2+}) of the amphibole experimental products for the 1 kbar experiments at 700 °C and above. There is a linear variation with a high correlation coefficient between the f_{H_2} and the oxidation state of Fe in the amphibole. The results for the GM buffer at 700 and 800 °C plot at the highest f_{H_2} values shown in the figure. If those values were on the order of 0.3–0.6 log units lower than shown, as suggested by Chou (1987a), the slopes of the 700 and 800 °C curves would be in somewhat better agreement with those at the higher temperatures.

A plot analogous to Figure 4 could be constructed for log f_{O_2} rather than log f_{H_2}, but H_2, not O_2, is the volatile species that controls equilibrium in the Fe oxy-substitu-

tion mechanism (Eq. 1) and, thus, is the critical variable in determining the oxidation state of Fe in these amphiboles. This conclusion is also supported by several experiments at the GM buffer, in which the capsule failed during the experiment, resulting in the loss of H_2O. In those experiments, the amphibole was exposed to essentially a CH_4-H_2 fluid phase with f_{H_2} fixed at that of the GM buffer. The Fe^{3+}/Fe_{tot} ratios of the resulting amphiboles were identical with the equilibrium values obtained at the same f_{H_2} but in the H_2O-H_2-O_2 fluid. Thus, the oxy-amphibole content is fixed by f_{H_2} and is independent of both f_{O_2} and f_{H_2O}. In both experimental and natural systems, f_{H_2}, f_{O_2}, and f_{H_2O} are interrelated by the dissociation reaction of H_2O and the total fluid pressure. Thus, f_{O_2} and f_{H_2O} affect the H-content and oxidation state of Fe in the amphibole only to the extent that they affect f_{H_2}.

It is evident from the 900 °C, 1–10 kbar results listed in Table 3 that Fe^{3+}/Fe_{tot} in amphibole decreases with increasing pressure at constant temperature and buffer assemblage. The effect of pressure can be quantified by means of the equilibrium constant for the oxidation-dehydrogenation reaction, as discussed below.

THERMODYNAMIC MODELS

Whereas the regression curves shown in Figure 4 can be used to predict precise f_{H_2} values from knowledge of Fe^{3+}/Fe^{2+} for the Vulcan's Throne amphibole sample, if the results of this study are to be applied to mantle-derived amphiboles with other chemical compositions, it is necessary to define the equilibrium constant (K) for the oxidation-dehydrogenation reaction represented by Equation 1. The partitioning of Fe and other major elements between amphibole and coexisting melt or solid phases can produce significant variation in the bulk chemical composition of kaersutitic amphiboles (e.g., see Popp and Bryndzia, 1992). However, the reaction described in Equation 1 does not involve solid components other than those within the amphibole. Therefore, if a value for the equilibrium constant for Reaction 1, as well as the proper activity-composition relations for the amphibole solid solution, can be determined, the results should be applicable to kaersutite of any bulk composition, regardless of the enclosing bulk rock or melt composition and regardless of the identity or chemical composition of coexisting mineral phases. Because other mineral phases are not involved in Equilibrium 1, the K values defined by experiments on a single-phase amphibole system can be applied to natural amphiboles in much more complex systems.

The log form of the equilibrium constant for Reaction 1 at constant T and P can be expressed by

$$\log K = \log f_{H_2} + \log a \qquad (2)$$

where a represents the activity product of the relevant chemical species in the amphibole. It follows from Equation 2 that
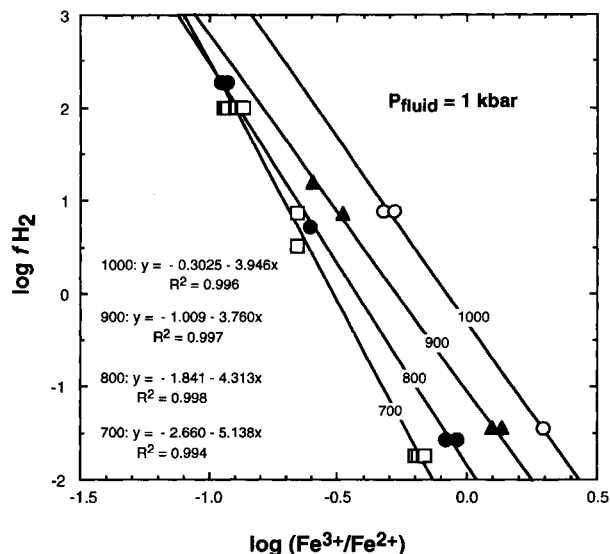

Fig. 4. Plot of log f_{H_2} vs. log (Fe^{3+}/Fe^{2+}) for 1 kbar experiments. Equations and curves for each temperature were obtained from linear least-squares fits. Temperatures are in degrees Celsius.

$$\frac{\delta \log f_{H_2}}{\delta \log a} = \frac{\delta \log K}{\delta \log a} - \frac{\delta \log a}{\delta \log a} = -1. \qquad (3)$$

Therefore, a slope of -1.0 results in the regression of log f_{H_2} against the expression for the amphibole activity term. The slopes obtained in the regression of $\log(Fe^{3+}/Fe^{2+})$ vs. log f_{H_2} (3.7–5.1 in Fig. 4) differ significantly from -1.0 and, thus, confirm that Fe^{3+}/Fe^{2+} does not represent the correct amphibole activity term.

To define the correct expression for the equilibrium constant, the oxidation-dehydrogenation reaction is written for a pair of Fe end-member calcic amphiboles such that

$$Ca_2Fe_5^{2+}Si_8O_{22}(OH)_2 = Ca_2Fe_3^{2+}Fe_2^{3+}Si_8O_{24} + H_2O. \qquad (4)$$
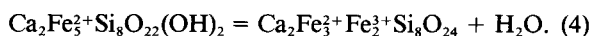
Reaction 4 represents equilibrium between a single amphibole phase and a fluid phase, for which the equilibrium constant is given by

$$K = f_{H_2} \frac{a_{Fe^{3+}}^{prod} \, a_{Fe^{2+}}^{prod} \, a_{[]}^{prod}}{a_{Fe^{2+}}^{react} \, a_{OH}^{react}} \qquad (5)$$

where the a terms represent the activities of Fe^{3+} and Fe^{2+} in the product and reactant amphibole, the activity of OH in the reactant amphibole, and the activity of O3 crystallographic sites from which the H has been lost in the product amphibole (designated as [ ] to indicate an H vacancy). The relation between activity and composition in multisite mineral phases has been discussed by Thompson (1967), Kerrick and Darken (1975), Powell (1978), Price (1985), and Spear (1993). In the formulation of Price (1985), the activity of component A in site j in a solid solution is given by

$$a = \left(\frac{n_j}{n_{Aij}} X_A^j \right)^{n_{Aij}} \cdot \gamma_i^{n_{Aij}} \qquad (6)$$

TABLE 5. Equations used to obtain Fe^{3+} and Fe^{2+} site populations

	Fe^{2+}			Fe^{3+}	
Site	a	b	Site	a	b
700 °C, 1 kbar					
M1	0.310	−0.327	M2	−0.005	0.398
M3	0.374	−0.353	M1	−0.047	0.441
M2	0.318	−0.324	M3	−0.033	0.251
800 °C, 1 kbar					
M1	0.335	−0.363	M2	−0.018	0.488
M3	0.399	−0.471	M1	−0.043	0.448
M2	0.266	−0.166	M3	−0.031	0.161
900 °C, 1 kbar					
M1	0.347	−0.296	M2	−0.054	0.684
M3	0.292	−0.233	M1	−0.053	0.368
M2	0.367	−0.478	M3	−0.031	0.161
1000 °C, 1 kbar					
M1	0.449	−0.557	M2	0.145	0.264
M3	0.383	−0.381	M1	−0.140	0.528
M2	0.178	−0.088	M3	0.000	0.151

Note: percent occupancy = $a + b(Fe^{3+}/Fe_{tot})$.

where X^j_A is the mole fraction of component A on the j site in the solid solution, n_j is the number of j sites in one formula unit of the end-member, n_{Aij} is the number of A atoms on the j site in one formula unit of the end-member, and γ_i is the activity coefficient.

Three solid solution models were applied to the experimental results by calculating the values of K for each experiment at any given temperature and pressure. In the random mixing model, it was assumed that Fe^{3+} and Fe^{2+} in both the reactant and product amphiboles in Reaction 4 mix randomly on the five octahedral sites (two M1, two M2, and one M3 site pfu), such that Fe^{3+}/Fe_{tot} is the same on all sites and OH and [ ] mix randomly on the two O3 sites. Thus, K is given by

$$K = f_{H_2} \frac{(\frac{5}{2} X_{Fe^{3+}})^2 (\frac{5}{3} X_{Fe^{2+}})^3 (X_{[]})^2}{(X_{Fe^{2+}})^5 (X_{OH})^2} \cdot \frac{(\gamma_{Fe^{3+}})^2 (\gamma_{Fe^{2+}})^3 (\gamma_{[]})^2}{(\gamma_{Fe^{2+}})^5 (\gamma_{OH})^2}. \quad (7)$$

Equation 7 can be reduced to

$$K = f_{H_2}(28.94) \frac{(X_{Fe^{3+}})^2 (X_{[]})^2}{(X_{Fe^{2+}})^2 (X_{OH})^2} \cdot \Phi \quad (8)$$

where Φ represents the activity coefficient term.

The nonrandom mixing model treated each of the octahedral M1, M2, and M3 sites individually but assumed that Fe^{3+} and Fe^{2+} mix randomly on all those sites in the end-member amphiboles, such that

$$K = f_{H_2}(28.94) \frac{(X^{M1}_{Fe^{3+}})^{0.8} (X^{M2}_{Fe^{3+}})^{0.8} (X^{M3}_{Fe^{3+}})^{0.4} (X_{[]})^2}{(X^{M1}_{Fe^{2+}})^{0.8} (X^{M2}_{Fe^{2+}})^{0.8} (X^{M3}_{Fe^{2+}})^{0.4} (X_{OH})^2} \cdot \Phi. \quad (9)$$

To obtain the mole fractions of Fe^{3+} and Fe^{2+} in the solid solutions, the Fe^{3+} and Fe^{2+} site occupancies determined by ^{57}Fe Mössbauer spectroscopy were used. In the observed ordering schemes, Fe^{3+}/Fe_{tot} varies among the three types of sites. Table 5 summarizes the equations used to predict the site occupancies as a function of Fe^{3+}/Fe_{tot} at 1 kbar. The equations give site occupancies that are in very good agreement with those estimated from X-ray diffraction measurements (M. W. Phillips, 1994 personal communication). A manuscript that discusses the Mössbauer spectroscopy and X-ray diffraction results is presently in preparation (Phillips et al., in preparation).

In the third solid solution model, Fe^{3+} and Fe^{2+} were considered to be ordered in the product end-member oxyamphibole in Reaction 4. The Fe^{3+}-Fe^{2+} distribution in the oxy-end-member was estimated by extrapolating the ordering schemes in Table 5 to the pure Fe end-member. The model produced a slightly better fit to the experimental data than the nonrandom mixing model at 700 °C but was not significantly different at higher temperatures. The model has an additional disadvantage in that the different site populations in the oxy-end-member at different temperatures require, in effect, that a different standard state be used at each temperature. Such a sliding-scale standard state complicates extrapolation or interpolation to temperatures other than those of the experiments. Because this model was not a significant improvement over the nonrandom mixing model, it is not considered further.

From Equations 8 and 9, a value of K can be calculated from the log f_{H_2}, H-content, and Fe^{3+}/Fe_{tot} values from each experiment that attained equilibrium (Table 3). Because H-contents were not measured on all the amphibole experimental products, OH and [ ] apfu in the O3 crystallographic site were taken to be (2.0 − Fe^{3+} − Ti) and (Fe^{3+} + Ti), respectively. Those terms follow from the results of Virgo et al. (1994), who documented that in kaersutitic amphibole, the sum of OH + Fe^{3+} + Ti = 2.0

TABLE 6. Goodness-of-fit and mean values for equilibrium constant expressions

T-P conditions	log (Fe^{3+}/Fe^{2+})		Random-mixing model		Non-random mixing model	
	Slope*	Mean log K**	Slope*	Mean log K**	Slope*	Mean log K**
700 °C, 1 kbar	−5.1(0.29)	0.20(1.4)	−1.90(0.02)	−0.173(0.56)	−1.14(0.12)	−0.605(0.25)
800 °C, 1 kbar	−4.3(0.31)	−0.02(1.3)	−1.58(0.02)	0.163(0.44)	−1.01(0.05)	−0.393(0.11)
900 °C, 1 kbar	−3.8(0.55)	−0.41(1.1)	−1.30(0.01)	0.377(0.18)	−0.92(0.08)	0.026(0.10)
1000 °C, 1 kbar	−3.9	−0.30(0.87)	−1.36(0.01)	0.950(0.22)	−1.19(0.05)	0.89(0.14)
900 °C, 5 kbar	−4.7	0.26(0.99)	−1.58	1.12(0.44)	−1.4	0.89(0.37)
900 °C, 10 kbar	−4.6	0.63(0.92)	−1.57	1.38(0.43)	−1.5	1.19(0.38)

* Slope of regression line for log f_{H_2} vs. log a_{amph}. See text for discussion. Number in parentheses is uncertainty at 95% confidence level. Uncertainty is not reported for conditions at which only two experiments were carried out.
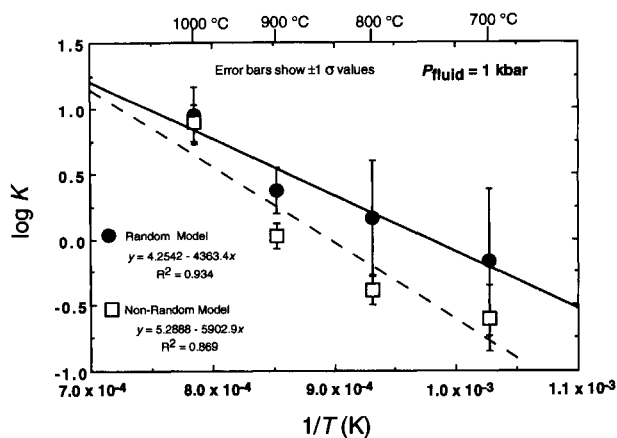** Number in parentheses represents ±1σ.

Fig. 5. Variation in log K for Reaction 4 vs. $1/T$ (K) for 1 kbar amphibole experimental products. Solid circles and solid line refer to K values calculated from the random mixing model; open squares and dashed line refer to K values calculated from the nonrandom mixing model. Error bars represent $\pm 1\sigma$ as given in Table 6. Straight lines and equations are from linear regression.

Fig. 6. Variation in log K for Reaction 4 vs. P (kbar) for 900 °C amphibole experimental products. Solid circles and solid line refer to K values calculated from the random mixing model; open squares and dashed line refer to K values calculated from the nonrandom mixing model. Error bars represent $\pm 1\sigma$ as given in Table 6. Straight lines and equations are from linear regression. The dot-dash line shows the theoretical slope calculated from the change in volume accompanying the oxidation-dehydrogenation reaction (see text).

apfu. The agreement between the calculated OH contents and the OH contents measured by H analysis of the experimental products is excellent (Virgo et al., 1994). In order to minimize the experimental uncertainties, values of log f_{H_2} and Fe^{3+}/Fe_{tot} were obtained at each temperature from the equations representing the best-fit least squares line in Figure 4. In the absence of information on the activity coefficients in chemically complex amphiboles such as these, the activity coefficient term in Equations 8 and 9 is ignored. The effect of ignoring the term is addressed in more detail below. The goodness-of-fit of the K expressions can be evaluated from the slope of the regression of log f_{H_2} vs. the amphibole activity term. As discussed above, a slope of -1.0 will result if the correct activity term is used. In addition, an identical value of log K will be obtained from each experiment at fixed T-P conditions. Table 6 summarizes the slopes of the log-log regression, as well as the mean and 1σ values of log K, for each of the experimental T-P conditions.

It is evident from Table 6 that both the random and nonrandom mixing models represent a much better approximation to the equilibrium constant than does the simple log(Fe^{3+}/Fe^{2+}) expression. For the 1 kbar results, the slopes for the random model decrease systematically from -1.90 at 700 °C to -1.30 and -1.36 at 900 and 1000 °C, respectively. For the 1 kbar results, the slopes of the log-log variation obtained from the nonrandom model are nearly identical, within the uncertainty limits, to the theoretical value of -1.0.

It is perhaps surprising that the activity coefficient term in Equations 8 and 9 can be essentially ignored for a chemically complex phase such as the Vulcan's Throne amphibole. It should be noted, however, that the Fe^{3+} and Fe^{2+} activities, as well as the OH and [ ] activities in Equations 8 and 9, refer to ions in the same set of crys-
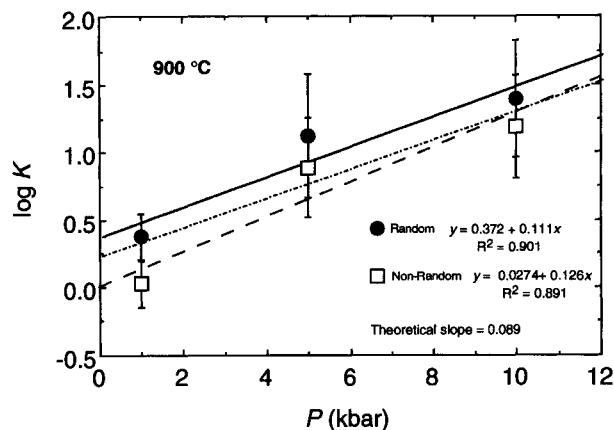
tallographic sites in the same mineral phase. Thus, the likelihood that the terms will cancel may be greater than for equilibria involving chemical species in two or more different mineral phases. A plot of log K vs. $1/T$ for the 1 kbar data for each of the mixing models is shown in Figure 5.

Effect of pressure

Values of log K, calculated from both of the mixing models, for the 900 °C experiments at 1, 5, and 10 kbar are plotted vs. pressure in Figure 6. The solid line represents a linear least squares fit to the data points for the random mixing model, whereas the dashed line represents the fit for the nonrandom mixing model.

The variation in log K as a function of pressure is defined by (e.g., Eugster and Skippen, 1967)

$$\Delta \log K = -\frac{\Delta V_s^0}{2.303RT}\Delta P \tag{10}$$

where ΔV_s^0 is the change in the standard state volume of the solid phases in Reaction 4, which in this case is simply the volume difference between the oxy- and hydroxy-Fe end-members. That volume difference at room temperature was estimated to be -19.5 (± 1.3) cm^3/mol on the basis of single-crystal X-ray diffraction measurements on a series of Vulcan's Throne samples treated at 700 °C and ranging in Fe^{3+}/Fe_{tot} from ~ 0.0 to 1.0 (Virgo et al., 1994; Phillips et al., in preparation). The dot-dash line in Figure 6 shows the theoretical slope for the pressure dependence calculated from Equation 10. The agreement between the observed and calculated slopes is reasonably good, given the uncertainty of the best-fit slope. An increase in temperature between room temperature (~ 25

TABLE 7. Difference between observed and calculated log f_{H_2} values for experiments

T-P conditions	Random* mixing model	Non-random* mixing model	Random** mixing model	Non-random** mixing model
700 °C, 1 kbar	0.59	0.28	0.56	0.26
800 °C, 1 kbar	0.43	0.26	0.44	0.17
900 °C, 1 kbar	0.27	0.31	0.33	0.11
1000 °C, 1 kbar	0.27	0.10	0.27	0.14
900 °C, 5 kbar	0.46	0.34	0.46	0.34
900 °C, 10 kbar	0.42	0.27	0.42	0.30

Note: numbers indicate mean absolute differences between the observed and calculated log f_{H_2} (i.e., |obs − calc|) for all experiments at each set of temperature-pressure conditions.
* Log K values used to calculate log f_{H_2} were obtained from Equations 11 and 12.
** Log K values used to calculate log f_{H_2} were taken from Table 6.

°C) and 900 °C should produce a slightly larger ΔV_s^0, which would, in turn, improve the agreement between the observed and theoretical slopes.

The log-log regression slopes for the 5 and 10 kbar experiments are given in Table 6. The somewhat poorer agreement with the theoretical value of −1.0 is considered to result from the smaller number of experiments at those pressures.

Summary

From the best-fit curves in Figures 5 and 6, it is possible to derive an equation from which values of K for Reaction 4 can be calculated at desired P-T conditions from either of the mixing models:

Random mixing model

$$\log K = 4.25 - 4363/T\ (\text{K}) + 0.11(P - 1)\ (\text{kbar}). \tag{11}$$

Nonrandom mixing model

$$\log K = 5.29 - 5903/T\ (\text{K}) + 0.13(P - 1)\ (\text{kbar}). \tag{12}$$

The log K values provide a means to predict equilibrium values of f_{H_2} from the Fe^{3+}/Fe_{tot} ratios of the amphibole. In order to evaluate the accuracy with which the log f_{H_2} can be estimated, the Fe^{3+}/Fe_{tot} values obtained in the experiments were used to calculate the corresponding f_{H_2} values from the log K values obtained from (a) the best-fit equations (11 and 12) and (b) the mean log K values reported in Table 6. The results are shown in Table 7, which gives the mean absolute differences between the calculated and observed log f_{H_2} values. From the random mixing model, the log f_{H_2} values can be predicted to within ~0.5 log units, whereas from the nonrandom mixing model, the log f_{H_2} values can be predicted to within ~0.33 log units.

In summary, the composition of kaersutitic amphibole can be a quite sensitive indicator of the f_{H_2} in the environment of formation, provided that the temperature and pressure are known. Either of the mixing models provides a reasonably accurate and precise estimate of the f_{H_2} at

which kaersutitic amphiboles have equilibrated. The nonrandom mixing model provides somewhat better estimates than the random mixing model but requires knowledge of the Fe site populations. Most of the analytical data that relates to natural kaersutitic amphiboles do not report site occupancies. In the absence of this information, the random mixing model must be used to make inferences about f_{H_2}.

It should be noted that the presence of Fe^{2+} in the M4 crystallographic site has been ignored in the equilibrium constant expressions, but the X-ray crystal structure refinement of the Vulcan's Throne sample suggests that up to ~0.12 Fe^{2+} may reside in M4 (Phillips et al., in preparation). Given the excellent fit of the nonrandom mixing model (Table 6), this simplification is apparently not significant.

Equilibrium constant Expressions 8 and 9 should apply, in general, to any calcic amphibole in which Fe^{3+} and Fe^{2+} mix on the five M1, M2, and M3 crystallographic sites. The chemical compositions of calcic amphiboles can be more complex because of variations in the A-site content, the Na content in the M4 site, and the [4]Al content. The equilibrium constants in Expressions 8 and 9 can be modified to include activity terms for those substitutions (e.g., Powell, 1978). However, Equilibrium 4 refers to chemical equilibrium within a single mineral phase that accommodates both the reactant and product amphibole species. Thus, any activity terms necessary to account for species such as [4]Al would have to be applied to both the reactant and product amphiboles and, therefore, would cancel in the K expression. Modifications to the equilibrium constant would be required if the cation partitioning in the tetrahedral and octahedral sites were different in the product and reactant amphiboles. In such a case, the additional terms in the equilibrium constant might not cancel.

APPLICATIONS

The results of the experimental study have both general and specific applications to understanding the petrological implications of naturally occurring kaersutitic amphiboles. Implicit in any attempt to infer conditions of formation from the compositions of naturally occurring amphibole assemblages is the requirement that the Fe^{3+}-Fe^{2+} ratio has not been altered by post-crystallization processes. In this connection, Dyar et al. (1993) have recently concluded that rates of H loss from amphiboles are such that pristine Fe^{3+}/Fe_{tot} values are likely to be retained on the time scales required for transport and emplacement of mantle-derived amphibole megacrysts to the surface. That conclusion was based on data for H-diffusion in amphibole (Graham et al., 1984) as applied to megacryst samples with grain sizes "on the order of 10 mm."

Use of Fe^{3+}-Fe^{2+} ratio to infer conditions of formation

Previous attempts to infer petrogenetic information from the oxidation state of Fe in kaersutitic amphiboles have generally relied on the Fe^{3+}-Fe^{2+} ratio expressed as

either Fe^{3+}/Fe_{tot} or Fe^{3+}/Fe^{2+} (e.g., Boettcher and O'Neil, 1980; McGuire et al., 1991; Popp and Bryndzia, 1992; Dyar et al., 1993; Righter and Carmichael, 1993). However, these variables do not represent the complete expression for the equilibrium constant. It follows from either of the equilibrium constant expressions, 8 or 9, that at any given temperature and pressure, the proportion of the O3 sites occupied by OH and [ ] exerts control over the Fe^{3+}-Fe^{2+} ratio. At constant f_{H_2}, an increase in the proportion of OH requires a corresponding increase in Fe^{3+}/Fe^{2+} in order for equilibrium to be maintained. For a given Fe^{3+}-Fe^{2+} ratio, OH content varies in relation to both the Ti-content and Fe_{tot} content. Sample calculations reveal that at fixed T and P, the variations in Ti and Fe_{tot} observed in natural kaersutite (Popp and Bryndzia, 1992) can produce variations in Fe^{3+}/Fe_{tot} of up to 0.3 at the f_{H_2} equivalent to the FMQ buffer. Thus, it is imperative that the complete expression for the equilibrium constant, rather than simply Fe^{3+}-Fe^{2+} ratio, be used in petrogenetic applications.

Temperature-f_{H_2}-Fe^{3+}/Fe_{tot} relationships for the Vulcan's Throne sample

From the best-fit linear equations shown in Figure 4, the equilibrium log f_{H_2}-T stability relations for the specific Vulcan's Throne amphibole composition can be calculated. Figure 7 shows contours of Fe^{3+}/Fe_{tot} within the amphibole subsolidus stability field for $P_{fluid} = 1$ kbar. For reference, the log f_{H_2}-T variation of the buffer curves for $P_{fluid} = 1$ kbar is also shown. Two somewhat unexpected results regarding the general behavior of Fe oxy-component lead to the conclusion that it is not necessary to appeal to post-crystallization oxidation to produce relatively high Fe^{3+}-Fe^{2+} ratios. Rather, high Fe^{3+}/Fe_{tot} values can reflect the operation of the oxy-substitution mechanism described in Reaction 1 within the stability field of the amphibole under subsurface conditions.

First, the effect of closed-system cooling on a melt-entrained amphibole favors the reduction, rather than the oxidation, of Fe. In Figure 7, the contours of constant Fe^{3+}/Fe_{tot} in amphibole are not parallel to the buffer curves, in contrast to melts and whole-rock systems (e.g., Carmichael, 1991). Therefore, if a rock or melt containing kaersutite undergoes closed-system cooling along a path parallel to a buffer curve, Fe^{3+}/Fe_{tot} in the amphibole decreases rather than increases. That is, if the kinetics of H-diffusion were to be rapid enough to produce a change in oxidation state, the Fe becomes more reduced rather than more oxidized as the system cools.

Second, kaersutitic amphiboles with relatively high proportions of Fe^{3+} can be stable at redox conditions generally considered to be typical for mantle-generated melts. Oxygen fugacities of mantle-derived melts and mineral assemblages are commonly considered to lie within approximately ±2–3 log units of the NNO buffer curve, but fugacities up to that of HM have been estimated in some cases (e.g., Bryndzia and Wood, 1990; Carmichael and Ghiorso, 1990; Carmichael, 1991; Righter and Carmichael, 1993). The corresponding range of Fe^{3+}/Fe_{tot} in the
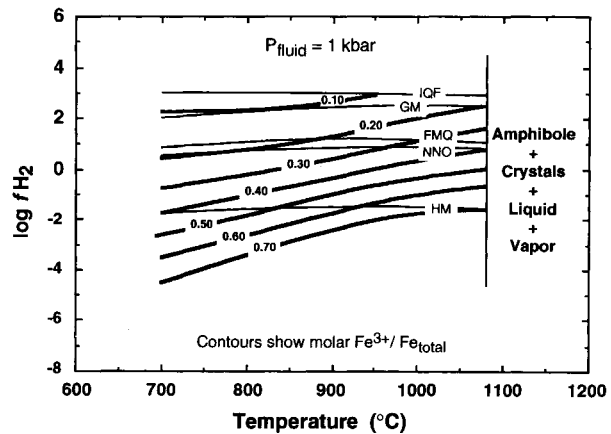

Fig. 7. Variation in Fe^{3+}-Fe^{2+} ratio of the Vulcan's Throne amphibole as a function of f_{H_2} and temperature within the subsolidus stability field. Contours of Fe^{3+}/Fe_{tot} (thick lines) were calculated from the equations in Fig. 4. Variation of f_{H_2} for the buffer curves (thin lines) was obtained from values given in Table 3. The relations depicted apply only to an amphibole with the Fe_{tot} and Ti content of the Vulcan's Throne sample.

Vulcan's Throne amphibole at solidus temperatures in Figure 7 is approximately 0.20–0.70. It is likely, however, that conditions of $P_{fluid} < P_{tot}$ prevails in the environment of formation of kaersutitic amphibole in the mantle. From the definition of H_2O activity (Eq. 13) and the dissociation constant of H_2O (Eq. 14)

$$a_{H_2O} = \frac{f_{H_2O,T\text{-}P}}{f_{H_2O,pure\text{-}T\text{-}P}} \tag{13}$$

$$K_{H_2O} = \frac{f_{H_2}(f_{O_2})^{1/2}}{f_{H_2O}} \tag{14}$$

it follows that at fixed f_{O_2} (as is the case for the buffer assemblages) a decrease in a_{H_2O} relative to that in the $P_{fluid} = P_{tot}$ system decreases f_{H_2} in 1:1 proportions. Thus, the effect of decreasing a_{H_2O} in a plot such as Figure 7 is to decrease the f_{H_2} of each of the buffer assemblages, while the contours of amphibole composition remain fixed. In other words, the Fe^{3+}/Fe_{tot} in amphibole at any given buffer increases as a_{H_2O} decreases. Thus, amphiboles with high Fe^{3+}-Fe^{2+} ratios can be stable at f_{O_2} equivalent to relatively reducing buffers if the activity of H_2O is low. The relation between H_2O activity and amphibole composition is discussed further below.

Estimation of f_{H_2} and a_{H_2O} from natural kaersutite compositions

If Fe^{3+}, Fe^{2+}, OH, and [ ] contents are known for kaersutite, the equilibrium constant for the random mixing model can be used to infer differences in f_{H_2} values between amphibole assemblages assumed to have equilibrated at the same temperature and pressure conditions, even if the actual values for T and P are unknown. Furthermore, if the temperature and pressure of amphibole equilibration can be estimated, the absolute f_{H_2} in the environment of amphibole formation can be calculated.

TABLE 8. Comparison of calculated log f_{H_2} for amphiboles from Dish Hill, California (McGuire et al., 1991, Table 6)

	Obs. Fe^{3+}/Fe_{tot}	Δ log f_{H_2}*
Sample Ba-2-1		
Selvage amphibole	0.70	
Interstitial amphiboles:		
WR-1	0.84	0.00
WR-2	0.82	-0.26
WR-3	0.86	0.00
WR-5	0.85	-0.16
Sample DH101		
Selvage amphibole	0.84	
Interstitial amphiboles:		
B	0.88	-0.50
C	0.91	-0.28
D	0.88	-0.59
E	0.90	-0.43

* The Δ log f_{H_2} refers to the difference between the calculated log f_{H_2} values of the selvage and interstitial samples, i.e., selvage value minus interstitial value.

McGuire et al. (1991) reported chemical analyses for amphibole, spinel, olivine, orthopyroxene, and clinopyroxene in two composite xenoliths from Dish Hill, California. They reported significant differences in Fe^{3+}/Fe_{tot} values between an amphibole selvage and the interstitial amphiboles at distances up to ~16 cm from the selvage. The two types of amphiboles, however, have significantly different Ti and Fe_{tot} contents, which result in different OH and [ ] contents. If it is assumed that both types of amphibole formed at the same temperature and pressure, the difference between f_{H_2} values of the assemblages can be calculated. The actual value of log K used in the calculations is arbitrary, because differences that result from variations in the amphibole mole fraction terms are independent of the numerical value of K. The results of such calculations for the Dish Hill amphiboles are reported in Table 8. For the Ba-2-1 sample, within the errors of measurement assumed to be on the order of 3% (relative), the selvage and interstitial amphiboles have equilibrated at essentially the same f_{H_2}. For the DH101 sample, f_{H_2} of the interstitial amphiboles range from 0.28 to 0.59 log units higher than those of the selvage amphibole. That is, even though Fe^{3+}/Fe_{tot} values of the interstitial amphiboles are higher than that of the selvage amphibole, the differences in OH and [ ] are such that higher f_{H_2} is required for the interstitial samples.

Figure 8 is a frequency histogram of equilibrium log f_{H_2} calculated for each kaersutite reported by Popp and Bryndzia (1992) and by Dyar et al. (1993), for which H contents were measured. The temperature and pressure of formation were taken to be 900 °C and 15 kbar, respectively, which are reasonable conditions for the equilibration of xenolith assemblages (e.g., Wood and Banno, 1973; Wood et al., 1990). The effect of P-T variations typical of mantle conditions, as described in the figure caption, are likely to shift the log f_{H_2} values by <1 log unit. Shown for reference is the variation in log f_{H_2} for the HM and FMQ buffers as a function of H_2O activities
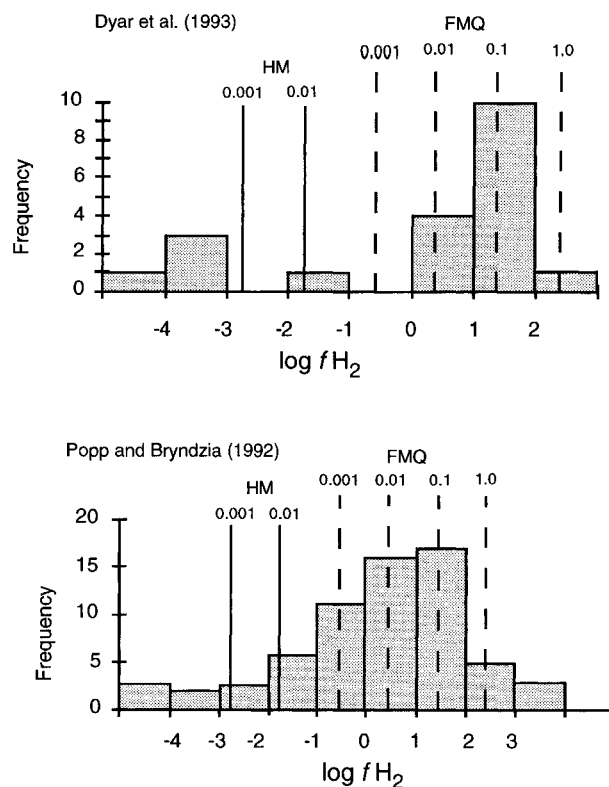

Fig. 8. Frequency histogram of calculated equilibrium log f_{H_2} for natural amphibole samples, assuming conditions of formation were 900 °C and 15 kbar. (top) Analyses reported by Dyar et al. (1993); (bottom) literature analyses compiled by Popp and Bryndzia (1992). The vertical dashed lines represent log f_{H_2} of the FMQ buffer for H_2O activities varying from 1.0 to 0.001. Solid vertical lines represent log f_{H_2} of the HM buffer for H_2O activities of 0.01 and 0.001. Effect of P-T uncertainties: increase in pressure shifts the log f_{H_2} to more positive values by 0.11 log units/kbar; increase in temperature shifts the log f_{H_2} to more positive values by ~0.5 log units/100 °C.

ranging from 0.001 to 1.0. The activities are calculated relative to the system in which $P_{fluid} = 15$ kbar $= P_{H_2O} + P_{H_2} + P_{O_2}$. The distribution of values in Figure 8 suggests that the majority of amphiboles could have formed under conditions near the FMQ buffer at relatively low H_2O activities, but several samples in each population yield relatively low log f_{H_2} values. Whether those amphiboles have been affected by post-crystallization oxidation-dehydrogenation or represent mantle conditions that have not previously been documented cannot be determined.

The compositional data reported for clinopyroxene, orthopyroxene, spinel, and amphibole from the Dish Hill locality by McGuire et al. (1991) provide sufficient information to calculate the temperature, f_{O_2}, f_{H_2}, and a_{H_2O} of formation of the xenolith assemblages, as summarized in Table 9. It is emphasized that even though the Fe^{3+}/Fe_{tot} values of the amphiboles are quite high (in the range 0.70–0.91), the f_{O_2} of the samples lies within approximately 1 log unit of the FMQ buffer. The relatively low f_{H_2} re-

TABLE 9. Estimates of temperature, f_{O_2}, f_{H_2}, and a_{H_2O} for xenoliths from Dish Hill

Sample	Ba-2-1	DH101
T (°C)*	1019(9)	931(5)
log f_{O_2}**	−9.53(0.22)	−9.86(0.22)
log f_{O_2} FMQ†	−9.53	−10.88
log f_{H_2}‡	0.01(0.15)	−0.64(0.13)
f_{H_2O} (bar)§	211(95)	159(75)
log a_{H_2O}‖	−2.42(0.21)	−2.54(0.21)

Note: mineral compositions reported by McGuire et al. (1991) were used for all calculations. Values in table represent mean of four assemblages from each xenolith. Pressure assumed to be 15 kbar. Numbers in parentheses are 1σ.
* Based on clinopyroxene + orthopyroxene geothermometry (Wells, 1977; Wood and Banno, 1973).
** Based on spinel peridotite O_2 barometer (Wood et al., 1990).
† Calculated from equation of Chou (1987b).
‡ Calculated from log K value obtained from Eqs. 8 and 11.
§ Calculated from Eq. 14.
‖ Calculated from Eq. 13.

quired for the high Fe^{3+} contents reflect relatively low H_2O activities in the environment. The calculated log a_{H_2O} values for the two Dish Hill samples are −2.4 and −2.5. Although there is little quantitative documentation of a_{H_2O} for mantle derived melts and mineral assemblages, Bell (1994; 1994 personal communication) has determined log a_{H_2O} in the range −2 to −3 based on the H contents of a suite of olivines from xenoliths entrained in alkali basalts from a number of localities. The low H_2O activities may represent low weight percent H_2O contents in the coexisting magmas under vapor-absent conditions. Alternately, under vapor-present conditions, low a_{H_2O} would result if H_2O represents only a small mole fraction of all species in a C-O-H fluid.

ACKNOWLEDGMENTS

REFERENCES CITED

Aoki, K. (1963) The kaersutites and oxykaersutites from alkalic rocks of Japan and surrounding areas. Journal of Petrology, 4, 198–210.
Bell, D.R., Rossman, G.R., Endisch, D., and Rauch, F. (1994) OH content of mantle olivine. Eos, 75, 230.
Best, M.G. (1970) Kaersutite-peridotite inclusions and kindred megacrysts in basanitic lavas, Grand Canyon, Arizona. Contributions to Mineralogy and Petrology, 27, 25–44.
——— (1974) Mantle-derived amphibole within inclusions in alkali basaltic lavas. Journal of Geophysical Research, 78, 2107–2113.
Binns, R.A., Duggan, M.B., and Wilkinson, J.F.G. (1970) High pressure megacrysts in alkaline lavas from north-eastern New South Wales. American Journal of Science, 269, 132–168.
Boettcher, A.L., and O'Neil, J.R. (1980) Stable isotope, chemical, and petrographic studies of high-pressure amphiboles and micas: Evidence for metasomatism in the mantle source regions of alkali basalts and kimberlites. American Journal of Science, 280A, 594–621.
Bryndzia, L.T., and Wood, B.J. (1990) Oxygen thermobarometry of abyssal spinel peridotites: The redox state of C-O-H volatile compositions of the Earth's sub-oceanic upper mantle. American Journal of Science, 290, 1093–1116.

Carmichael, I.S.E. (1991) The redox states of basic and silicic magmas: A reflection of their source regions? Contributions to Mineralogy and Petrology, 106, 129–141.
Carmichael, I.S.E., and Ghiorso, M.S. (1990) The effect of oxygen fugacity on the redox state of natural liquids and their crystallizing phases. In Mineralogical Society of America Reviews in Mineralogy, 24, 192–210.
Chou, I-M. (1987a) Calibration of the graphite-methane buffer using the f_{H_2} sensors at 2-kbar pressure. American Mineralogist, 72, 76–81.
——— (1987b) Oxygen buffer and hydrogen sensor techniques at elevated pressures and temperatures. In G.C. Ulmer and H.L. Barnes, Eds., Hydrothermal experimental techniques, 523 p. Wiley, New York.
Clowe, C.A., Popp, R.K., and Fritz, S.J. (1988) Experimental investigation of the effect of oxygen fugacity on ferric-ferrous ratios and unit-cell parameters in four natural clinoamphiboles. American Mineralogist, 73, 487–499.
Dawson, J.B. (1984) Contrasting types of upper mantle metasomatism. In Developments in Petrology, vol. 11: Kimberlites, p. 289–294. Elsevier Science, Amsterdam.
Dawson, J.B., and Smith, J.V. (1982) Upper mantle amphiboles: A review. Mineralogical Magazine, 45, 35–46.
Dyar, M.D., Mackwell, S.J., McGuire, A.V., Cross, L.R., and Robertson, J.D. (1993) Crystal chemistry of Fe^{3+} and H^+ in mantle kaersutite: Implications for mantle metasomatism. American Mineralogist, 78, 968–979.
Ernst, W.G. (1968) Amphiboles, 125 p. Springer-Verlag, New York.
Eugster, H.P., and Skippen, G.B. (1967) Igneous and metamorphic reactions involving gas equilibria. In P.H. Ableson, Ed., Researches in geochemistry, vol. 2, p. 492–520. Wiley, New York.
Francis, D.M. (1976) The origin of amphibole in lherzolite xenoliths from Nunivak Island, Alaska. Journal of Petrology, 17, 357–378.
Frey, F.A., and Prinz, M. (1978) Ultramafic inclusions from San Carlos, Arizona: Petrologic and geochemical data bearing on their petrogenesis. Earth and Planetary Science Letters, 38, 129–176.
Graham, C.M., Harmon, R.S., and Sheppard, S.M.F. (1984) Experimental hydrogen isotope studies: Hydrogen isotope exchange between amphibole and water. American Mineralogist, 69, 128–138.
Griffen, W.L., Wass, S.Y., and Hollis, J.D. (1984) Ultramafic xenoliths from Bullenmerri and Gnotuk Maars Victoria, Australia: Petrology of a subcontinental crust-mantle transition. Journal of Petrology, 25, 53–87.
Harte, B. (1983) Mantle peridotites and processes: The kimberlite sample. In C.J. Hawkesworth and M.J. Norry, Eds., Continental basalts and mantle xenoliths, p. 46–91. Shiva, Nantwich, U.K.
Harvey, R.P., and McSween, H.Y. (1992) The parent magma of the nakhlite meteorites: Clues from melt inclusions. Earth and Planetary Science Letters, 111, 467–482.
Helz, R.T. (1982) Experimental studies of amphibole stability: Phase relations and compositions of amphiboles produced in studies of the melting behavior of rocks. In Mineralogical Society of America Reviews in Mineralogy, 9B, 279–346.
Huckenholz, H.G., Gilbert, M.C., and Kunzman, T. (1992) Stability and phase relations of calcic amphiboles crystallized from magnesio-hastingsite compositions in the 1 to 45 kbar pressure range. Neues Jahrbuch für Mineralogie Abhandlungen, 164, 229–268.
Huebner, J.S. (1971) Buffering techniques for hydrostatic systems at elevated pressures. In G.C. Ulmer, Ed., Research techniques for high pressure and high temperature, p. 123–177. Springer-Verlag, New York.
Irving, A.J., and Frey, F.A. (1984) Trace element abundances in megacrysts and their host basalts: Constraints on partition coefficients and megacryst genesis. Geochimica et Cosmochimica Acta, 48, 1207–1221.
Johnson, M.C., Rutherford, M.J., and Hess, P.C. (1991) Cassigny petrogenesis: Melt compositions, intensive parameters, and water contents of Martian (?) magmas. Geochimica et Cosmochimica Acta, 55, 349–366.
Kerrick, D.M., and Darken, L.S. (1975) Statistical thermodynamic models for ideal oxide and silicate solid solutions, with applications to plagioclase. Geochimica et Cosmochimica Acta, 39, 1431–1442.
Kurat, G., Palme, H., Spettel, B., Baddenhausen, H., Hofmeister, H., and Wanke, H. (1980) Geochemistry of ultramafic xenoliths from Kapfenstein, Austria: Evidence for a variety of upper mantle processes. Geochimica et Cosmochimica Acta, 44, 45–60.

Lamb, W., and Valley, J.W. (1984) Low CO_2, vapor-absent metamorphism of reduced granulites. Nature, 312, 56–58.

Leake, B.E. (1968) A catalog of analyzed calciferous and subcalciferous amphiboles together with their nomenclature and associated minerals. Geological Society of America Special Papers, 98, 210 p.

McGuire, A.V., Dyar, M.D., and Nielson, J.E. (1991) Metasomatism of upper mantle peridotite. Contributions to Mineralogy and Petrology, 109, 252–264.

Merrill, R.B., and Wyllie, P.J. (1975) Kaersutite and kaersutite eclogite from Kakanuii, New Zealand: Water-excess and water-deficient melting to 30 kilobars. Geological Society of America Bulletin, 86, 555–570.

Nickel, K.G., and Green, D.H. (1984) The nature of the uppermost mantle beneath Victoria, Australia, as deduced from ultramafic xenoliths. In Developments in Petrology, vol. 11: Kimberlites, p. 159–178. Elsevier Science, Amsterdam.

Oba, T., Yagi, K., and Hariya, Y. (1983) Stability relations of kaersutite: A refinement. Proceedings, First International Symposium on Hydrothermal Reactions, 659–668.

Oxburgh, E.R. (1964) Petrological evidence of amphibole in the upper mantle and its petrogenetic and geophysical implications. Geological Magazine, 101, 1–19.

Phillips, M.W., Popp, R.K., and Clowe, C.A. (1991) A structural investigation of oxidation effects in air-heated grunerite. American Mineralogist, 76, 1502–1509.

Popp, R.K., and Bryndzia, L.T. (1992) Statistical analysis of Fe^{3+}, Ti, and OH in kaersutite from alkalic igneous rocks and mafic mantle xenoliths. American Mineralogist, 77, 1250–1257.

Popp, R.K., Virgo, D., Hoering, T.C., Yoder, H.S., and Phillips, M.W. (1993) Experimental study of oxy-component in kaersutitic amphibole. Geological Society of America Abstracts with Programs, 25, A-95.

Powell, R. (1978) Equilibrium thermodynamics in petrology, 284 p. Harper and Rowe, London.

Price, J.G. (1985) Ideal site mixing in solid solutions, with an application to two-feldspar geothermometry. American Mineralogist, 70, 696–701.

Redhammer, G.J., Beran, A., Dachs, E., and Amthauer, G. (1993) A Mössbauer and X-ray study of annites synthesized at different oxygen fugacities and crystal chemical implications. Physics and Chemistry of Minerals, 20, 382–394.

Righter, K., and Carmichael, I.S.E. (1993) Mega-xenocrysts in alkali olivine basalts: Fragments of disrupted mantle assemblages. American Mineralogist, 78, 1230–1245.

Robie, R.A., Hemingway, B.S., and Fisher, J.R. (1978) Thermodynamic properties of minerals and related substances at 298.15 K and 1 bar (10^5 Pascals) pressure and at higher temperatures. U.S. Geological Survey Bulletin 1452, 456 p.

Schneider, M.E., and Eggler, D.H. (1984) Compositions of fluids in equilibrium with peridotite: Implications for alkaline magmatism-metasomatism. In J. Kornprobst, Ed., Kimberlites: I. Kimberlites and related rocks, p. 384–394. Elsevier, Amsterdam.

Spear, F.S. (1993) Metamorphic phase equilibria and pressure-temperature-time paths, 799 p. Mineralogical Society of America Monograph, Washington, DC.

Stewart, D.C., Boettcher, A.L., and Eggler, D.H. (1979) Phase relations of kaersutite at upper mantle conditions: Implications for its subsolidus origin. Eos, 60, 418.

Thompson, J.B., Jr. (1967) Thermodynamic properties of simple solutions. In P.H. Ableson, Ed., Researches in geochemistry, vol. 2, p. 322–361. Wiley, New York.

Treiman, A.H. (1985) Amphibole and hercynite spinel in Shergotty and Zagami: Magmatic water, depth of crystallization, and metasomatism. Meteoritics, 20, 229–243.

Ulmer, G.C., Rosenhauer, M., Woermann, E., Ginder, J., Drory-Wolff, A., and Wasilewski, P. (1976) Applicability of electrochemical oxygen fugacity measurements to geothermometry. American Mineralogist, 61, 653–660.

Virgo, D., Young, E.D., Popp, R.K., Hoering, T.C., and Phillips, M.W. (1994) The petrological significance of exchange components in kaersutites: A statistical and experimental analysis. Fifth International Symposium, Experimental Mineralogy, Petrology, and Geochemistry, University College, London. Terra Abstracts, 6 (1), 50.

Wallace, M.E., and Green, D.H. (1991) The effect of bulk rock composition on the stability of amphibole in the upper mantle: Implications for solidus positions and mantle metasomatism. Mineralogy and Petrology, 44, 1–19.

Wells, P.R.A. (1977) Pyroxene thermometry in simple and complex systems. Contributions to Mineralogy and Petrology, 62, 129–139.

Wilkinson, J.F.G., and LeMaitre, R.W. (1987) Upper mantle amphiboles and micas, and TiO_2, K_2O, and P_2O_5 abundances, and 100Mg/(Mg + Fe^{2+}) ratios of common basalts and andesites: Implications for modal mantle metasomatism and undepleted mantle compositions. Journal of Petrology, 28, 37–73.

Wilshire, H.G., and Shervais, J.W. (1975) Al-augite and Cr-diopside ultramafic xenoliths in basaltic rocks from western United States: Structural and textural relationships. Physics and Chemistry of the Earth, 9, 257–272.

Wilshire, H.G., Meyer, C.E., Nakata, J.K., Calk, L.C., Shervais, J.W., Nielson, J.E., and Schwarzman, E.C. (1988) Mafic and ultramafic xenoliths from volcanic rocks of the western United States. U.S. Geological Survey Professional Paper, 1443, 170 p.

Wood, B.J., and Banno, S. (1973) Garnet-orthopyroxene and orthopyroxene-clinopyroxene relationships in simple and complex systems. Contributions to Mineralogy and Petrology, 42, 109–124.

Wood, B.J., Bryndzia, L.T., and Johnson, K.E. (1990) Mantle oxidation state and its relationship to tectonic environment and fluid speciation. Science, 248, 337–345.

Yoder, H.S., Jr. (1950) High-low quartz inversion up to 10,000 bars. Transactions of the American Geophysical Union, 31, 827–835.